RSC Advances

ROYAL SOCIETY OF CHEMISTRY

www.rsc.org/advances

Thermal-based regulation on biomineralization and biological properties of bioglass nanoparticles decorated PAN-based carbon nanofibers

Dan Cheng[a], Zhiwei Ren[a], Lijuan Guo[a], Cuihua Zhang[a], Xiaolong Jia[a,b,*], Qing Cai[a,c,*], Xiaoping Yang[a,b,c]

Abstract

Composite carbon nanofibers (CNFs) containing bioglass (BG) nanoparticles displayed different morphology and micro-structures depending on sintering temperatures (800, 1000 and 1200 ^{o}C) when they were produced from electrospun polyacrylonitirle-BG precursor blend nanofibers. Biomineralization using simulate body fluid (SBF) and biological evaluation using osteoblast culture were performed to investigate their relationship with sintering temperatures. Characterizations revealed that BG nanoparticles on CNF/BG sintered at 1000 ^{o}C (CNF/BG-1000) possessed small particle size and uniform size distribution, and the crystallinity of BG nanoparticles increased as the sintering temperature increasing from 800 to 1200 ^{o}C. The dissolution rate of BG nanoparticles was thus different between the cases, which enhanced the biomineralization and cell proliferation/differentiation in varying degrees. Benefiting from the homogeneous distribution and the large specific surface area of BG nanoparticles on CNFs, the results demonstrated that CNF/BG-1000 had the strongest ability in promoting apatite deposition, proliferation and osteogenic differentiation of MC3T3-E1 pre-osteoblasts in comparison with CNF/BG sintered at 800 or 1200 ^{o}C. The results suggested a flexible tool to regulate the physiochemical and biological properties of CNF/BG composites by controlling the sintering temperature, which could find promising application in skeleton repairing.

Keywords: bioactive glass nanoparticles; carbon nanofibers; biomineralization; cell proliferation; osteogenic differentiation.

1. Introduction

Carbon nanofibers (CNFs) have widely attracted considerable attention for both fundamental scientific research and their potential biomedical applications, due to their good mechanical properties, chemical stability, high aspect ratio and surface properties allowing for easy functionalization with biocompatible hydrophilic groups [1-4]. Specifically, CNFs have been increasingly applied in bone repairing since Webster's group reported that the adhesion and proliferation of osteoblasts were selectively enhanced by nano-scaled carbon fibers [5]. In order to achieve sufficient binding between CNFs and bone tissue, combinations of CNFs with other osteocompatible materials are envisioned very effective approaches. Bioactive glass (BG) is a kind of bioceramic materials, which has been long investigated for applications in bone regeneration. In addition to its excellent bone binding properties, soft connective tissues were also reported able to form a bind with BG, which led BG substrates bind firmly with living bone and surrounding tissues [6-10]. These characteristics of BG implied that the addition of BG into CNFs could enhance their abilities of bone binding and bone defect repairing in comparison to pure CNFs, as found in our previous works [11, 12]. Besides, composite CNFs containing BG component (CNF/BG) displayed a kind of "degradation" feature with the dissolution of BG, which would break down the continuous CNFs. On the other hand, the obtained CNF/BG composites had the advantage of high mechanical properties deriving from CNFs, and were able to offset the intrinsic drawback of poor strength of BG materials. Promisingly, CNF/BG composites could be used as substrates directly for cell culture or as bioactive reinforcements for other polymeric biomaterials.

The mechanism of bioactivity and bone binding ability of BG was attributed to the formation of mineralite layer (such as hydroxycarbonated apatite (HCA)) on its surface, a layer similar to the mineral part of bone, along with the chemical degradation of BG by releasing sodium, calcium and silicon ions, etc. when it was in contact with body fluid [13-15]. In the cases of CNF/BG composites, the dissolution-deposition and ion exchanging related to BG would be more complicated because of the combination of two completely different materials. It was reported in our previous works [16-19] and literatures [20, 21] that the physicochemical

properties and surface morphology of electrospun CNF/metal or CNF/metal oxide composites significantly depended on preparation parameters such as pre-oxidation conditions and sintering conditions. Arstila H. et al. reported that the chemical compositions and crystal types of BG varied remarkably with sintering temperatures [22]. Ma J. et al also found that the sintering temperature greatly influenced the structural feature of pure BG, which directly affected the biomineralization and bioactivity of BG [23]. Similarly, in our previous work [19], the morphology evolution, crystallization behavior and growth kinetics of BG component in CNF/BG composites were also found being determined by sintering temperature and time. The BG component in CNF/BG composites could be in the form of amorphous, wollastonite polycrystals or pseudowollastonite crystals, and it could exist inside the CNFs and/or on the surface of CNFs in different sizes and shapes. Marta G. C. et al. reported that the effects of BG on biomineralization and bone repairing were predominated by its physicochemical properties and surface morphology [24]. Julie E. G. et al. stated that the formation rate of mineralite layer was faster on BG with rough surface than that with smooth surface, and the large specific surface area of BG favored the adhesion and proliferation of osteoblasts [25]. With all these approaches, it could be thus deduced that the biomineralization and the bioactivity of CNF/BG composites would be strongly affected by their preparation parameters. Therefore, it was quite necessary to relate key preparation parameters (e.g. sintering temperature) of CNF/BG composites to their biological features, which would be very helpful in regulating the performance of CNF-based substrates in biomedical applications.

To this end, 58S type BG (mol %: 58.0 % SiO_2 - 26.3 % CaO - 15.7 % P_2O_5) was embedded into CNFs by using electrospinning and carbonization techniques similar to our previous works [11, 12, 16, 17, 19], which has been identified an efficient way to produce CNF/BG composites in laboratory. Briefly, polyacrylonitirle(PAN)/N,N-dimethylformamide(DMF) solution with addition of BG precursor sol-gel solution was electrospun and sintered at different temperatures to render CNFs with further flexibility in property regulation. The as-electrospun composite nanofibers were sintered at 800, 1000 or 1200 ^oC to obtain

CNF/BG composites with different morphology and structure as following our previous work [19]. Biomineralization in simulate body fluid (SBF) and in vitro osteoblast culture on CNF/BG composites were performed to investigate their dependence on the sintering temperature by evaluating the apatite formation, cell proliferation and osteogenic differentiation. A favorable hypothesis of the present study was that the changes in morphology and structure of CNF/BG composites could be a useful tool to regulate their biological features.

2. Experimental section

2.1 Materials

PAN (M_w = 100,000 g/mol), containing 93.0 wt.% acrylonitrile, 5.3 wt.% methylacrylate and 1.7 wt.% itaconic acid, was purchased from Courtaulds Co. (UK). BG precursors including triethyl phosphate (TEP), calcium nitrate tetrahydrate (CN) and tetraethoxysilane (TEOS) were purchased from Aldrich (USA) and used directly. DMF (99.5 %) was bought from Tianjin Fine Chemical Co. (China). Salts for preparation of SBF and other reagents required for the experiments were of analytically pure grade and obtained from Beijing Fine Chemical Co. (China).

2.2 Sample preparation

Referring to our previous works [11, 12, 19, 26], the preparation of CNF/BG composites was briefly described as follows. Firstly, TEP (10 ml) was dissolved in a mixed solvent containing absolute ethyl alcohol (10.12 ml), distilled water (3.16 ml) and ammonia water (0.12 ml) under stirring at 80 ^{o}C for 24 h to obtain a hydrolyzed TEP solution. Then, the hydrolyzed TEP solution (0.155 ml), CN (0.42 g) and TEOS (0. 65 ml) were added in turn into 20 ml of DMF, in which, 10 wt% of PAN had been dissolved in advance. The system was stirred continuously at room temperature for 48 h to obtain a homogeneous solution for electrospinning. Electrospinning was conducted at parameters as 15 kV (voltage), 0.3 mL/h (flow rate) and receiving distance (15 cm), using a rolling rod as the collector. The as-spun nanofibers were stabilized at 280 ^{o}C in air for 0.5 h,

then sintered at 800, 1000 or 1200 °C for 3 h in N_2 atmosphere to obtain the CNF/BG composites. For clarity, CNF/BG composites sintered at 800, 1000 and 1200 °C were named in terms of CNF/BG-800, CNF/BG-1000 and CNF/BG-1200, accordingly. The BG type in the CNF/BG composites was 58S type with chemical composition of 58 % SiO_2-33 % CaO-9 % P_2O_5 in mole as the aforementioned feeding dose shown. Pure CNF sheet was prepared in a similar way except the addition of BG precursors and the sintering condition was set as 1000 °C /3 h.

2.3 Biomineralization

Biomineralization in vitro is usually applied to evaluate bone binding ability of substrates for bone repairing. Therefore, CNF/BG composites were soaked in 1.5 times SBF (1.5SBF), which contained nearly 1.5 times of the inorganic ion concentrations of human blood plasma. The 1.5SBF was prepared by dissolving reagent grade salts (NaCl, $NaHCO_3$, Na_2SO_4, KCl, $K_2HPO_4{\cdot}3H_2O$, $MgCl_2{\cdot}6H_2O$, and $CaCl_2{\cdot}2H_2O$) in 1 L distilled water, and the final concentrations of ions were 213.0 mM Na^+, 7.5 mM K^+, 3.8 mM Ca^{2+}, 2.3 mM Mg^{2+}, 221.7 mM Cl^-, 6.3 mM HCO_3^-, 1.5 mM HPO_4^{2-} and 0.8 mM SO_4^{2-}, respectively. The solution pH was adjusted to 7.4 at 37±0.2 °C with the buffer solution (0.05 mol/L) composed of tris(hydroxymethyl)aminomethane (Tris) and hydrochloric acid. CNF/BG composite sheets were cut into patches (2 cm×4 cm) and immersed in the 1.5SBF at 37±0.2 °C for 0.5 day, 1 day, 3 days, 5 days, 7 days and 14 days. At each predetermined time point, samples were retrieved and gently rinsed with distilled water, and then freeze-dried for 24 h.

2.4 Biological properties

In order to evaluate the biocompatibility and cell affinity of CNF/BG composites, a mouse calvaria-derived osteoblast cell line (MC3T3-E1) was used for cell culture and seeding. The cells were cultured in Dulbecco's Modified Eagle Medium (DMEM, Hyclone, USA) supplemented with 10 % fetal bovine serum (FBS, PAA, Germany), 100 IU/ml penicillin (Sigma, USA) and 100 mg/ml streptomycin (Sigma, USA) in an incubator

(Sanyo, Japan) with 5 % CO_2 at 37 ^oC and saturated humidity. When having grown to confluence of 80 %, MC3T3-E1 cells were digested by 0.25 % trypsin (Sigma, USA) and 0.02 % ethylene diaminetetraacetic acid (EDTA) for further use.

Cell proliferation. Circular CNF/BG or pure CNF sheets (Φ□□□10 mm) were fixed into 48-well tissue culture plates, followed by sterilizing 4 h with UV exposure. After being rinsed by PBS for twice, MC3T3-E1 suspensions were added into each well at a density of 1×10^4 cells/well, and subsequently cultured at 37 °C in a humidified 5 % CO_2 with the medium refreshed every 2 days. Cell proliferation was tested by Cell Counting Kit-8 (CCK-8, Beyotime, China). CCK-8 is a kind of yellow solution which can be reduced to orange by active cells, whose absorbance is directly proportional to cell number. Briefly, at day 1, 3, 5 and 7 after cell seeding, 20 μl of CCK-8 solution was added into each well and incubated for 4 h, and then the OD value was measured at 490 nm (Bio-Rad 580). Cell number was calculated by a standard curve.

Cell morphology. At day 1, 3, 5 and 7 after cell seeding, cell-material complexes were collected and rinsed three times with PBS, and then fixed with 2.5 % glutaraldehyde solution (Beijing Chemical Plant, China). The fixed samples were dehydrated with graded ethanol solutions (30, 50, 70, 80, 90 and 100 %) and air-dried overnight for SEM observation.

ALP activity. For osteogenic differentiation assay, cell density of 5×10^4 for each well was applied. Cell-material complexes were incubated in osteogenic medium, containing 0.05 mmol/L vitamin C (Sigma, USA), 10 mmol/L β-sodium glycerophosphate (Sigma, USA) and 1×10^{-8} mol/L dexamethasone (Sigma, USA), for 3, 7, 14 and 21 days. Then they were retrieved from the culture plate and rinsed by PBS for three times. Cells were lysated by 1 % Triton X-100, and the alkaline phosphatase (ALP) activity of lysate was tested by *p*-nitrophenyl phosphate (*p*-NPP, Amerisco, USA). Aliquots of cell lysate were incubated with 5 mmol/L *p*-NPP in 0.1 mol/L glycine-KOH solution (pH = 10.5) for 0.5 h at 37 °C, and the reaction was stopped by KOH solution. OD values were measured by a microreader (Bio-rad 680, USA) at 405 nm. The relative ALP activity was represented as OD value/cell number ratio.

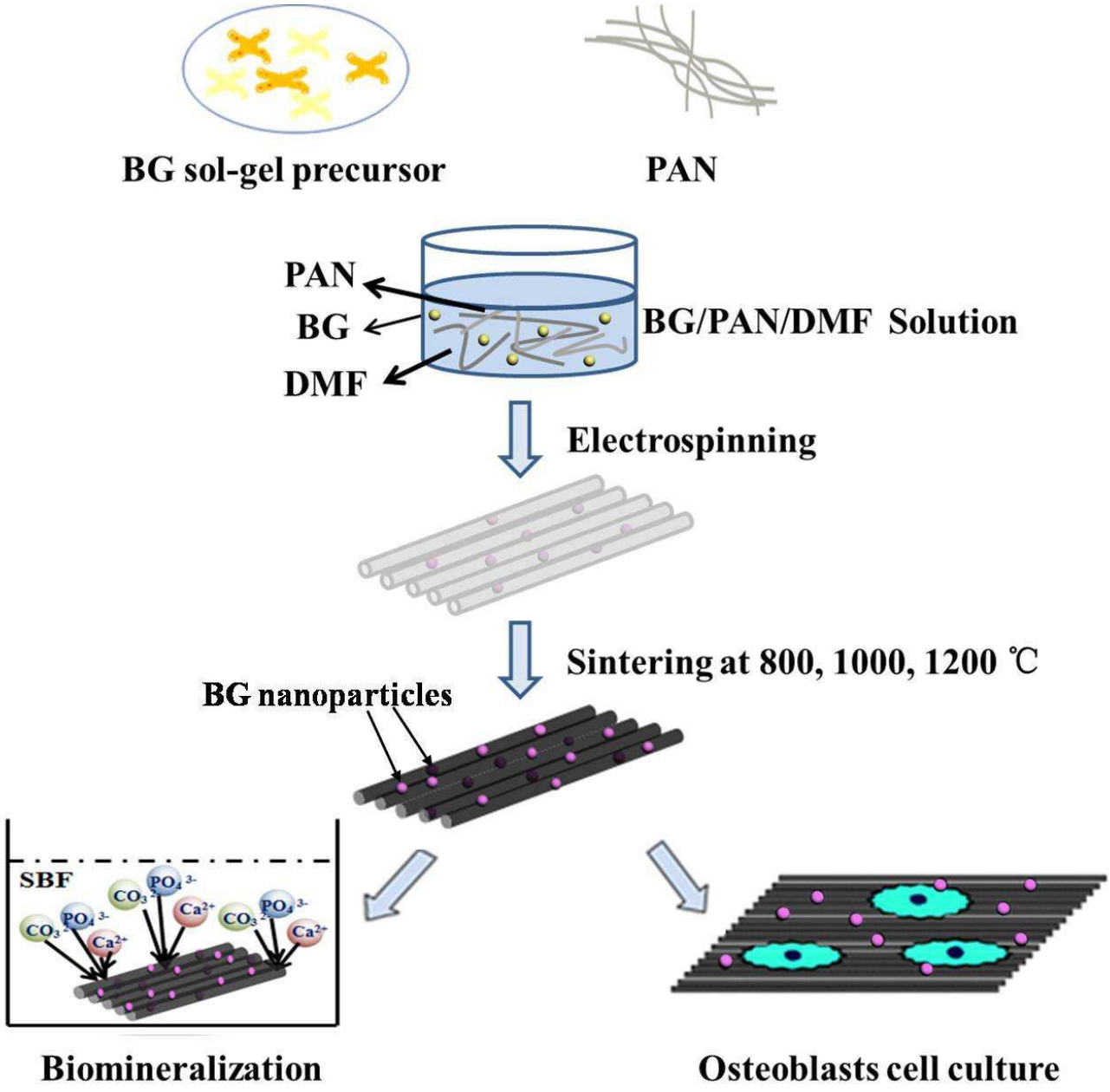

Fig. 1 Schematic illustration of experimental process.

2.4 Characterizations

The morphology of both nanofibers and cells was observed by scanning electron microscope (SEM, S-250, UK) at an accelerating voltage of 15-20 kV and transmission electron microscopy (TEM, JEOL 2000 EX, Japan) at an accelerating voltage of 200 kV. Before SEM observation, the sample surface was coated with a thin layer of a gold alloy (30 mA, 20 s) using a sputter coater (E5600, Polaron, USA). For TEM examination,

the samples were firstly dispersed in ethanol under ultrasonication and mounted onto formvar carbon coated 100 mesh nickel grids. Average fiber diameters and particle sizes were calculated with SEM images by using ImageJ software (National Institutes of Health, USA) to measure at least 500 nanofibers or nanoparticles. Crystalline microstructures of CNFs and BG nanoparticles were investigated by high resolution transmission electron microscope (HR-TEM, Hitachi H-800, Japan) at an operating voltage of 200 kV. The contents of BG component in CNF/BG composites were determined by themogravimetric analysis (TGA, TA, Q-50) at a heating rate of 10 ^{o}C /min towards 750 ^{o}C in air atmosphere. Chemical compositions were determined by energy dispersive spectroscopy (EDS, 51-ADD0011, USA) and Fourier transform infra-red spectroscopy (FT-IR, Magna 750R, Nicolet, USA). The X-ray diffraction patterns were collected using an X-ray diffractometer with Cu K-radiation (XRD, Rigaku D/max 2500 VB2+/PC) operating at 40 kV and 200 mA.

2.5 Statistical analysis

The experiments of biological property evaluation were performed in triplicate (n = 3) and repeated for three times. The results were presented as mean ± SD. Statistical analysis was made by *t*-test between two groups and the differences were considered as significant for $p \leq 0.05$.

3. Results and discussion

3.1 Characterizations of CNF/BG composites

Fig. 2 shows SEM, TEM and HR-TEM images of CNF/BG composites sintered at various temperatures. Parallel-aligned fibrous matrixes were obtained in all cases because a rolling rod was used as the receiver in electrospinning. It could be seen from the images that visible nanoparticles existed both outside and inside the CNFs at the same time, which were the BG nanoparticles according to our previous works [11, 12, 19, 26]. The amounts of the loaded BG nanoparticles in the three CNF composites were all around 9.5 wt.%, as measured by TGA (Fig. 3(a)), and were held consistent due to their similar fabrication process. As shown in Fig. 2(a_1, a_2), numerous BG nanoparticles with average size of 42 nm were observed within the fibers and

only a few nanoparticles were found on the fiber surface for CNF/BG-800. For CNF/BG-1000, a mass of spherical nanoparticles with average size of 75 nm covered fiber surface evenly with a small amount of nanoparticles inside the fiber (Fig. 2(b_1, b_2)). Similar phenomenon was observed for CNF/BG-1200, as shown in Fig. 2(c_1, c_2), but nanoparticles had merged into cuboid-like geometry with average size of 107 nm and sparse particles could be found inside the fiber. As reported in our previous work [19], BG nanoparticles in CNF/BG-800 were amorphous, whereas nanoparticles in CNF/BG-1000 were mainly composed of wollastonite (β-$CaSiO_3$) polycrystals and those in CNF/BG-1200 mainly consisted of pseudowollastonite ($Ca_3(Si_3O_9)$) single crystals. This was characterized and confirmed with HRTEM (Fig. 2(a_3, b_3, c_3) and XRD (Fig. 3(b)). In FFT patterns, no diffraction spot or ring was found for CNF/BG-800, while the diffraction spots in different patterns for CNF/BG-1000 and CNF/BG-1200 indicated the two materials having crystalline domains but in different crystalline structures. Also, the HRTEM images revealed the same results that no clear lattice fringe could be found for CNF/BG-800, while well-defined lattice fringes with an average d-spacing of 0.71 or 1.41 nm were clearly seen in the cases of CNF/BG-1000 and CNF/BG-1200, respectively. These two lattice fringes were suggested the formation of the (1 0 0) lattice plane of wollastonite structure [27] and the (1 0 1) lattice plane of pseudowollastonite structure [28]. The XRD results provided more solid evidences for this deduction. As shown in Fig. 3(b), no characteristic sharp peak was found in the XRD pattern of CNF/BG-800, except the broad and weak diffraction peaks at 2θ = 24.7° and 44.5° for the (0 0 2) and (1 0 1) reflections of graphitic carbon. Referring to the matching analysis of JADE software and literatures [29, 30] the peak at 2θ = 32.8° was assigned as the (1 0 0) reflection of wollastonite (β-$CaSiO_3$) (JCPDS 42-0547) in CNF/BG-1000, and the peak at 2θ = 31° was assigned as the (1 0 1) reflection of pseudowollastonite ($Ca_3(Si_3O_9)$) (JCPDS 74-0874) in CNF/BG-1200. Apparently, the produced CNF/BG composites from different sintering temperatures could have different morphological and structural characteristics, which evoked the interest to relate them to biomineralization and biological response targeting for bone repairing applications.

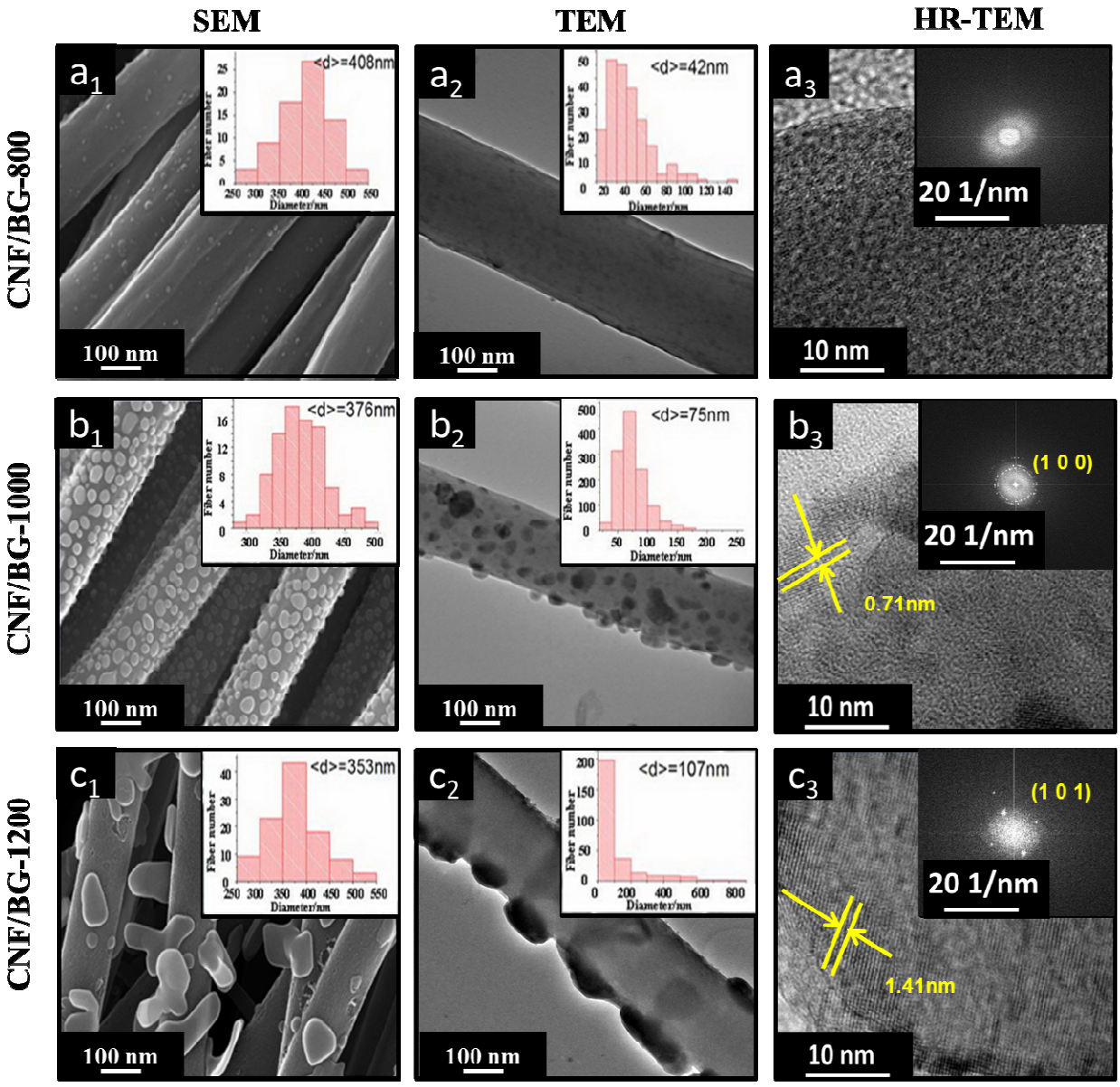

Fig. 2 SEM (left column), TEM (mid column) and HRTEM (right column) images of (a_1-a_3) CNF/BG-800, (b_1-b_3) CNF/BG-1000 and (c_1-c_3) CNF/BG-1200. The insets in SEM, TEM and HRTEM images are the diameter distribution of CNFs, the size distribution of BG nanoparticles and FFT images, respectively.

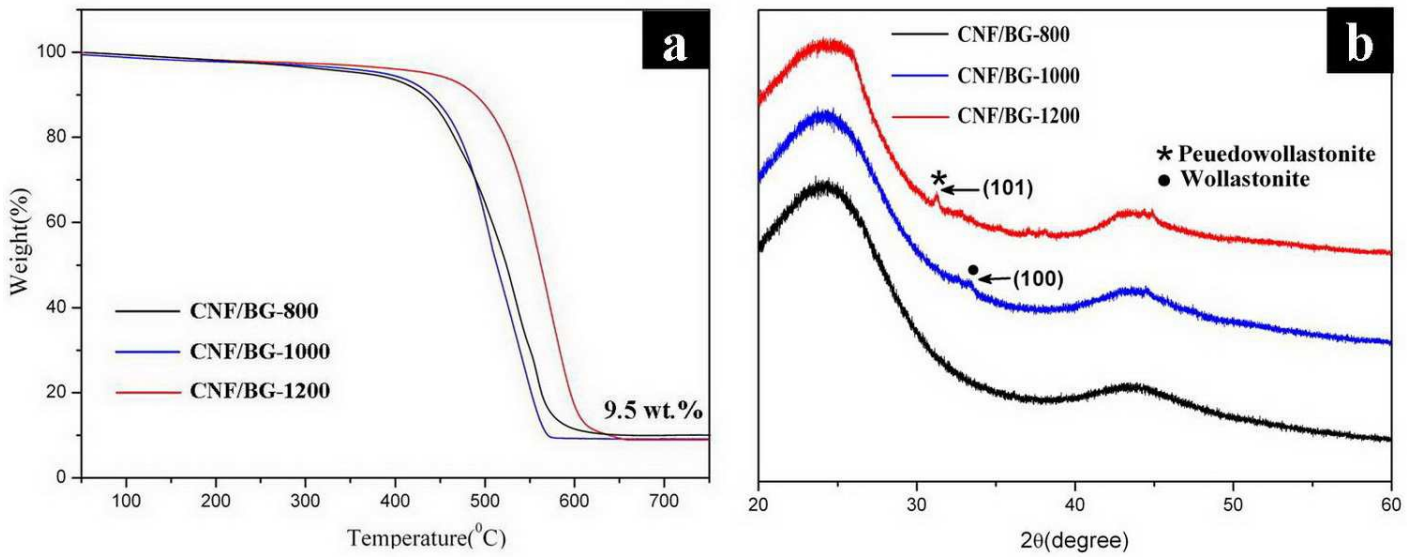

Fig. 3 (a) TGA curves and (b) XRD patterns of CNF/BG-800, CNF/BG-1000 and CNF/BG-1200.

3.2 Apatite deposition on CNF/BG composites in SBF

The ability of apatite formation in SBF has been identified useful and reasonable in evaluating osteocompatibility of biomaterials as if the mineralized nucleation was heterogeneous instead of homogeneous precipitation [31-33]. In reference to our previous works [12, 16, 17, 26], 1.5SBF was selected to perform the biomineralization for its supersaturation not high enough to cause homogeneous nucleation and the SBF able to remain transparent during the experiment. Fig. 4 shows SEM images obtained for different CNF/BG composites after being soaked in 1.5SBF for 0.5-14 days. Within only 0.5 day, it was found that the surfaces of all CNF/BG composites became much smoother in comparison with their original ones. Those BG nanoparticles on CNF surface had dissolved as they contacted with the SBF aqueous solution. However, the dissolution imprint of the BG particles could be tracked as shown in Fig. 4(a_1, b_1, c_1), that a spot of mineralites could be seen originating from where the original BG nanoparticles located. After 1 day soaking in the 1.5SBF, clusters of mineralite depositions were clearly detected on all the three CNF/BG composites, especially on CNF/BG-1000, which was almost covered completely by newly-formed mineralites (Fig. 4(a_2, b_2, c_2)). In our previous works [11, 12], CNF/BG composites had been confirmed having strong ability in

enhancing apatite deposition in comparison with pure CNFs by providing active sites with the dissolution of BG component. In the present case, the difference in mineralite deposition rate was inferred from the different dissolution rates of BG component in CNF/BG composites, because their morphology, particle size, distribution and crystalline structure differed from each other depending on sintering temperature. It seemed CNF/BG-1000 displaying the fast dissolution and ion-exchanging rate of BG and providing the most nucleation sites for mineralite deposition among the three CNF/BG composites, followed by CNF/BG-1200 and CNF/BG-800. As shown in Fig. 2, BG nanoparticles, being in the form of wollastonite polycrystals, were mainly on the surface of CNFs, which endowed them large effective contact area to SBF solution and led to fast dissolution. The BG nanoparticles in CNF/BG-800 were mainly amorphous, which should dissolve faster than those in CNF/BG-1000 theoretically. However, they were supposed to diffuse out of CNFs slowly because the BG component was dominantly embedded inside the fibers. While in the case of CNF/BG-1200, the exposed BG nanoparticles were found in the form of pseudowollastonite single crystals, which would slow down the dissolution rate of BG nanoparticles due to the higher crystallinity in comparison with the case of CNF/BG-1000. Thus, it was expected to find the biomineralization proceeding on CNF/BG composites in an order of CNF/BG-1000 > CNF/BG-1200 > CNF/BG-800 at the initial stage.

As the biomineralization going on, more and more mineralites deposited onto CNF/BG composites continuously (Fig. 4(a_3, b_3, c_3)). The original CNFs could be seen fully wrapped by mineralites when they were soaked in 1.5SBF for 7 days. And until the 14th day of biomineralization, the whole CNF/BG composites had been completely covered with a layer of mineralites (Fig. 4(a_4, b_4, c_4)). It was revealed that no distinct difference in morphology between different CNF/BG composites could be observed after soaking for a long time.

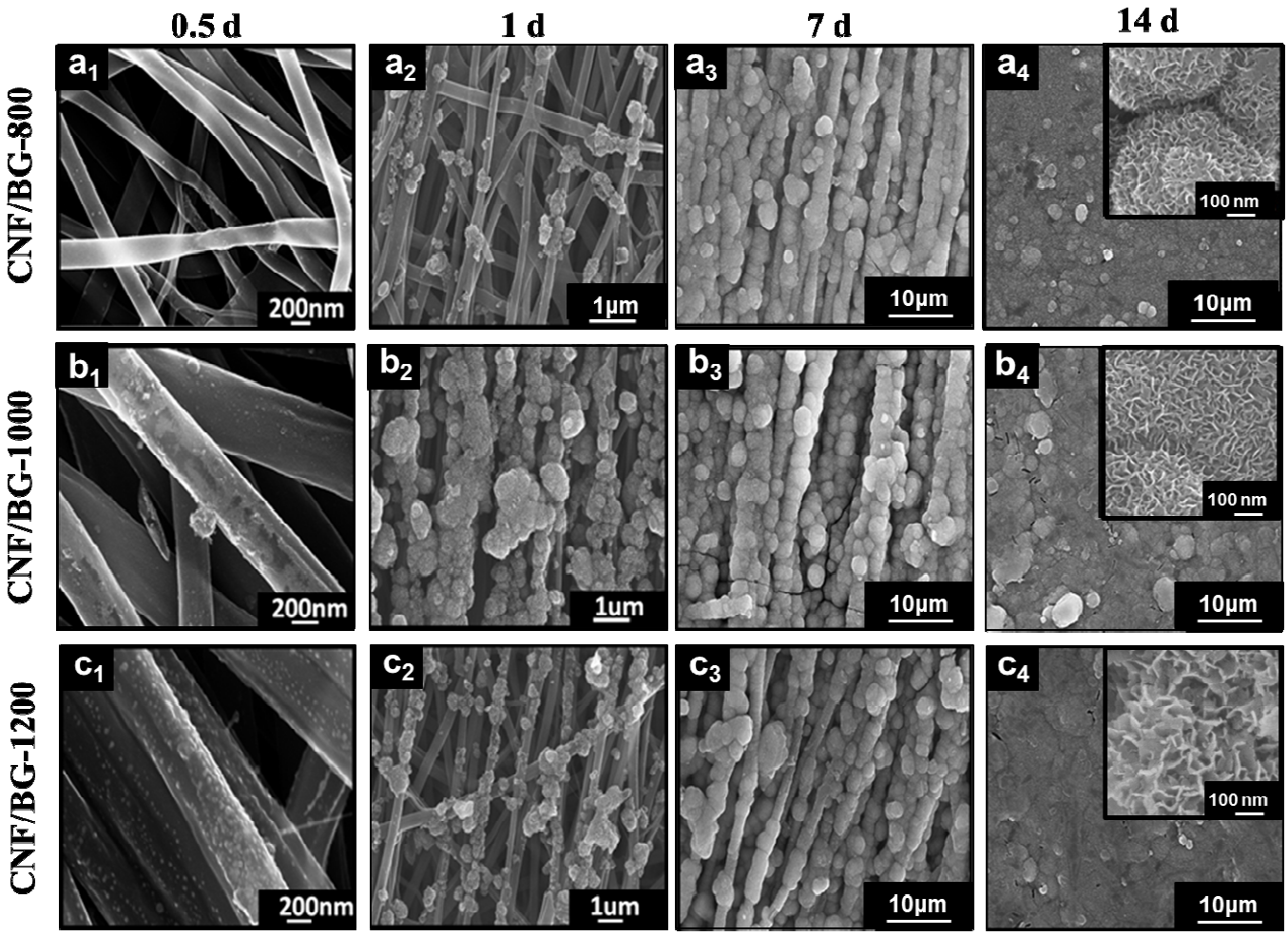

Fig. 4 SEM images for (a_1-a_4) CNF/BG-800, (b_1-b_4) CNF/BG-1000 and (c_1-c_4) CNF/BG-1200 after soaking in 1.5SBF for 0.5, 1, 7 and 14 d (from left to right) at 37 ^{o}C. The insets are the corresponding high-resolution images.

The images in Fig. 4 illustrated the mineralite depositions having a kind of flaky-like structure, which was identified the typical structure of crystalline hydroxyapatite (HA) [12, 35]. To confirm this inference, FT-IR and XRD analysis on biomineralized CNF/BG composites were carried out and the results are shown in Fig. 5. From FT-IR spectra (Fig. 5(a_1, b_1, c_1)), changes in chemical structures could be identified for all CNF/BG composites as the soaking time prolonging. The strengths of the absorption bands at 564, 961, 879 and 1036 cm^{-1} increased gradually with longer soaking time, and the signals were ascribed to the formation

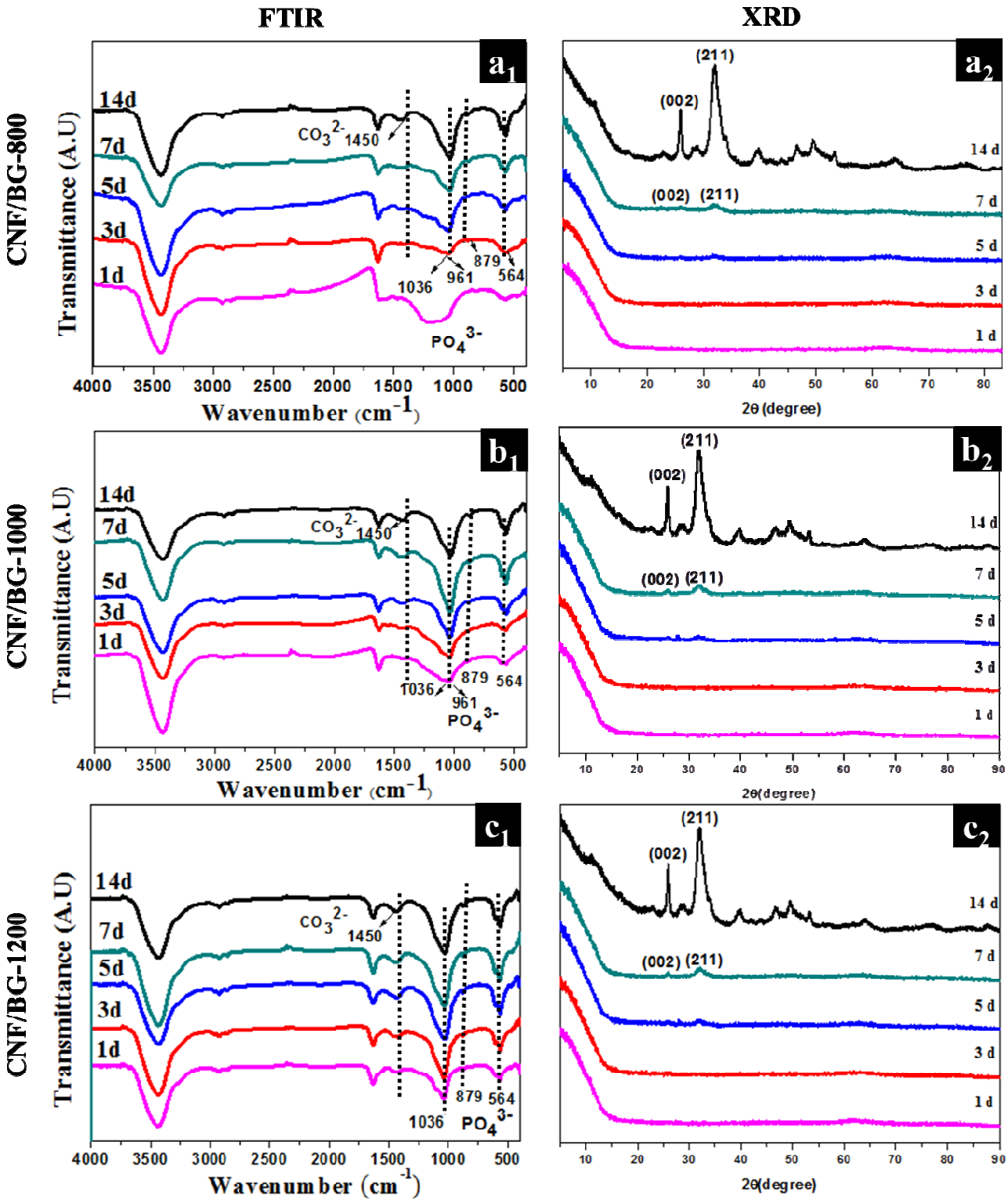

Fig.5 FTIR patterns (left column) and XRD spectra (right column) obtained for (a_1-a_2) CNF/BG-800, (b_1-b_2) CNF/BG-1000 and (c_1-c_2) CNF/BG-1200 after soaking in 1.5SBF at 37 °C for various time.

of PO_4^{3-} or HPO_4^{2-} groups [35]. The peak at 1450 cm^{-1} was attributed to the CO_3^{2-} [36], which implied the mineralite depositions being carbonated. Normally, the crystallinity of mineral depositions from SBF was not high due to their fast nucleation and growth rate. Observed from the XRD patterns (Fig. 5(a_2, b_2, c_2)), two weak diffraction peaks at $2\theta = 25^o$ and 32^o were detected after the materials had been soaked in the SBF for over 5 days. And the peaks were intensified remarkably with longer soaking time. Inferring from literatures [37-40], the two peaks were assigned to the crystal planes of (0 0 2) and (2 1 1) of HA, and the crystallinity of HA increased with its continuous deposition from the SBF to CNF/BG composites. Accompanied with the accumulating formation of HA on CNF/BG, changes in chemical compositions were also detected definitely by EDS. It could be seen from Fig. 6 that the contents of Si decreased, while those of Ca and P increased rapidly with SBF soaking. After 14 days of incubation, the deposited apatite displayed a Ca/P molar ratio of 1.63, which was close to the characteristic value (1.67) of stoichiometric HA [41].

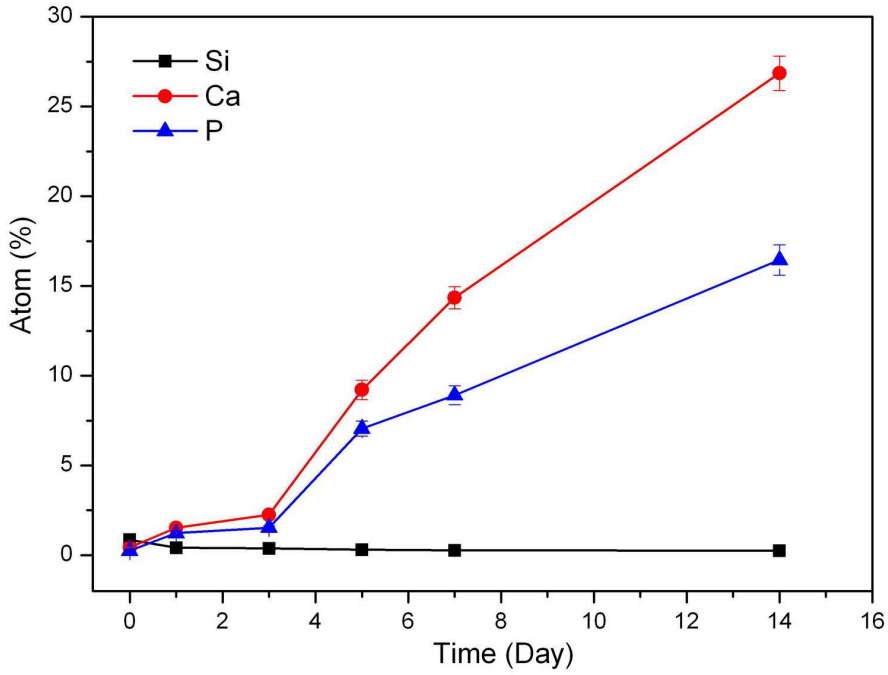

Fig. 6 EDS results obtained for CNF/BG-1000 after being soaked in 1.5SBF at 37 ^oC for various time.

Taking all the aforementioned results into account, it was clear that the apatite formation ability on CNF/BG composites originated from the dissolution of BG component, whose morphology and crystalline structure could affect its dissolution rate and the apatite deposition thereof. The sintering temperature could be a tool to regulate the location, the size and the crystalline structure of BG nanoparticles on CNFs. From Fig. 4, CNF/BG-1000 demonstrated the strongest ability in inducing apatite nucleation and growth, followed by CNF-1200 and CNF-800. Generally, it was believed that the initial ion-exchanging process was essential for inducing the apatite deposition when BG was soaked into aqueous solutions [38, 40]. The exchange of cationic ions (e.g. Ca^{2+} and Na^{+}) with H^{+} (or H_3O^{+}) ions would cause the solution pH increasing, which subsequently led to the hydrolysis of silica groups. Thus, active sites for apatite nucleation were generated, and an amorphous calcium phosphate (ACP) layer on the BG surface was formed at the initial stage by attracting Ca^{2+} and PO_4^{3-} ions from surrounding solution [42]. From Fig. 2 and Fig. 3, it had been known that CNF/BG-1000 displayed homogeneous distribution of BG nanoparticles densely packed on fiber surface, and the BG component was a kind of wollastonite (β-$CaSiO_3$) polycrystals. The BG nanoparticles were exposed to SBF sufficiently and dissolved fast in the SBF, which induced the fast nucleation and growth of apatite on CNF/BG-1000. The BG component in CNF/BG-800 was mainly amorphous, which dissolved faster than wollastonite-type BG. However, these BG nanoparticles were predominantly embedded inside the CNFs and had less chance in contacting with SBF than in the case of CNF/BG-1000. As for CNF/BG-1200, those BG nanoparticles on fiber surface had transformed into pseudowollastonite ($Ca_3(Si_3O_9)$) single crystalline structure, whose solubility was inferior to wollastonite due to its higher crystallinity. Besides, the size of BG nanoparticles in CNF/BG-1200 was also larger than that in CNF/BG-1000 so that the latter would have faster BG dissolution rate than the former due to the nano effect of particle size [43]. It was suggested that BG nanoparticles with smaller particle size had larger surface area, subsequently facilitating the contact of BG with SBF, which accelerated the dissolution of BG components. Therefore, in the present study, CNF/BG-1000 was found able to enhance the fastest apatite formation among the three CNF/BG composites.

3.3 *In vitro* osteoblast culture on CNF/BG composites

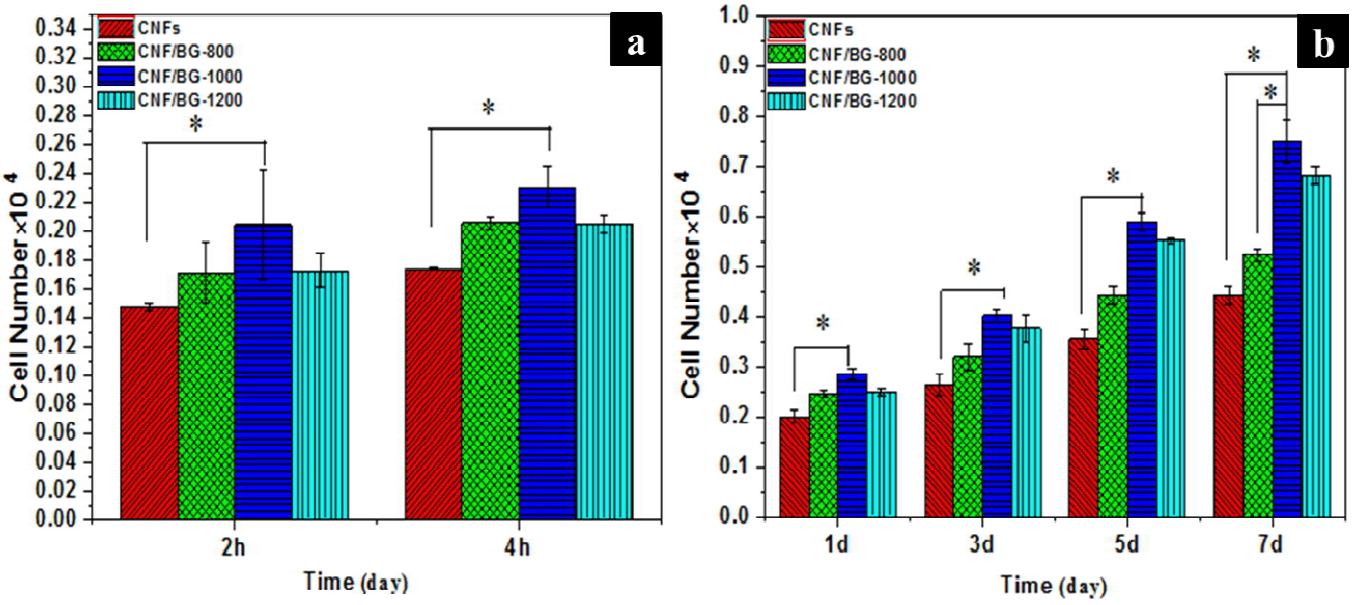

Fig. 7 (a) Adhesion and (b) proliferation of osteoblasts MC3T3-E1 on pure CNFs and CNF/BG for various time. The results are represented as mean ± standard deviation for n = 3 ($P < 0.05$).

By culturing osteoblasts MC3T3-E1 on composite CNFs, using pure CNFs as control, the osteocompatibility of CNF/BG composites was evaluated by cell adhesion, proliferation and osteogenic differentiation assessments, along with cell morphology observation. As shown in Fig. 7(a), cells had adhered onto all substrates at 2 h after cell seeding, and the cell adhesion slightly increased in all cases at the 4th hour after cell seeding. In comparison with pure CNFs, the cells could be seen more likely adhering onto CNF/BG composites at the same time point. The cell adhesion on CNF/BG-1000 was found the highest among the three CNF/BG composites. As the cell culture proceeding on, continuous growth in MC3T3-E1 cells was detected on all substrates, showing the materials not having obvious cytotoxicity and adverse effect on cell proliferation (Fig. 7(b)). While the cell proliferation rate differed significantly in different cases that cells grew the fastest on CNF/BG-1000, followed by CNF/BG-1200, CNF/BG-800 and finally pure CNFs. The cell proliferation was enhanced on CNF/BG composites in comparison with pure CNFs due to the

incorporation of bioactive component of BG. The trend in cell proliferation on the three CNF/BG composites was similar to that in biomineralization, which was suggested also relating to the dissolution rate of BG nanoparticles. Apparently, the released ions had played effective function in promoting cell proliferation. CNF/BG-1000, with the fastest dissolution rate of BG nanoparticles, displayed the highest cell affinity among the three CNF/BG composites.

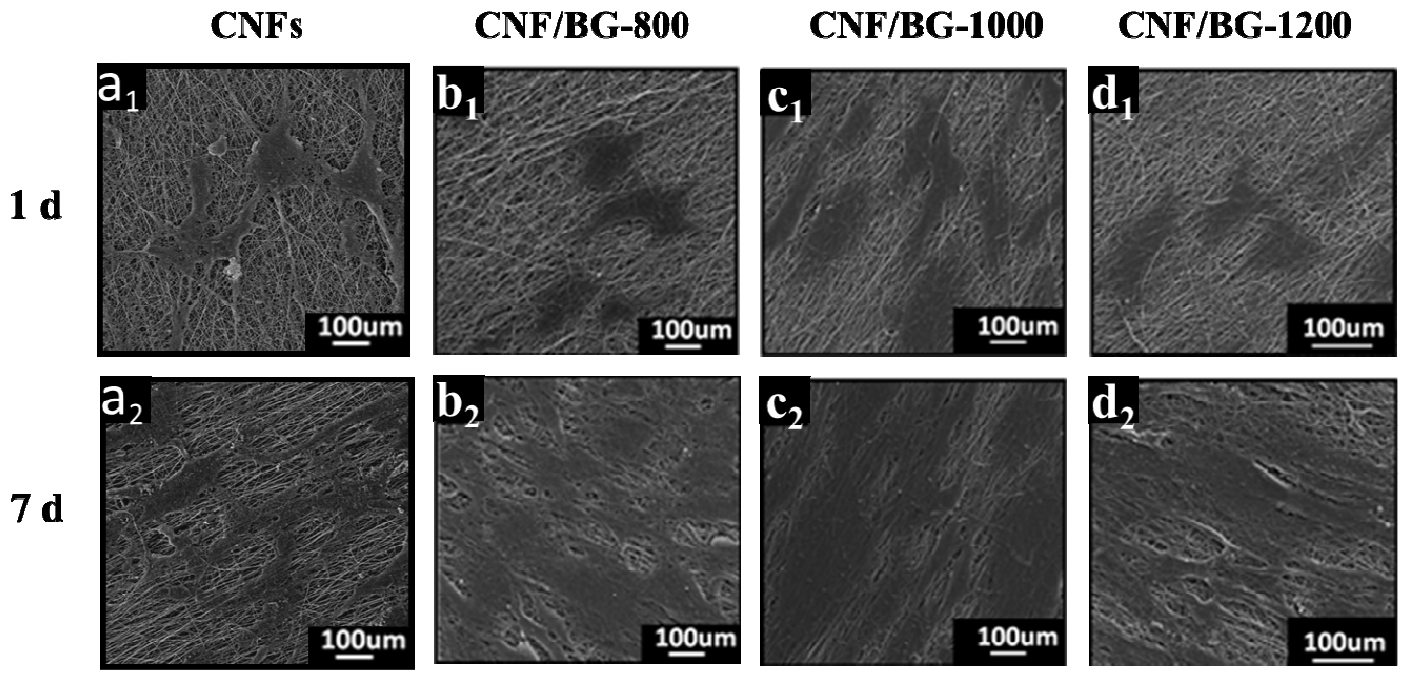

Fig. 8 SEM images of osteoblasts (MC3T3-E1) cultured on CNFs and CNF/BG (from left to right) for (a_1-d_1) 1 and (a_2-d_2) 7 d.

Morphology of cultured osteoblasts on pure CNFs and various CNF/BG composites was observed and shown in Fig. 8. On the first day after cell seeding, MC3T3-E1 cells could be seen having adhered onto all nanofibrous matrixes and spread. More cells were found on CNF/BG-1000 than the other three materials. When being cultured for 7 d, the proliferation of MC3T3-E1 cells was clearly identified as the images showing many confluent cells on substrates. In all the cases, the cells were in normal spindle-like morphology, displaying oriented growth along the fiber direction. The cells tended to elongate along fiber

direction because of the contact guide effect, which was a common phenomenon when cells were cultured on parallel-aligned fibrous matrixes [44, 45]. Rich extracellular matrix was synthesized and secreted to connect adjacent cells together, especially in the case of CNF/BG-1000, which was almost fully covered with confluent cells at the 7th day. The results confirmed that both pure CNFs and CNF/BG composites were biocompatible and affinitive to osteoblasts. The numerous BG nanoparticles on fiber surface of CNF/BG-1000 might have contributed much to its good ability in enhancing cell adhesion by providing active sites for cell grasping.

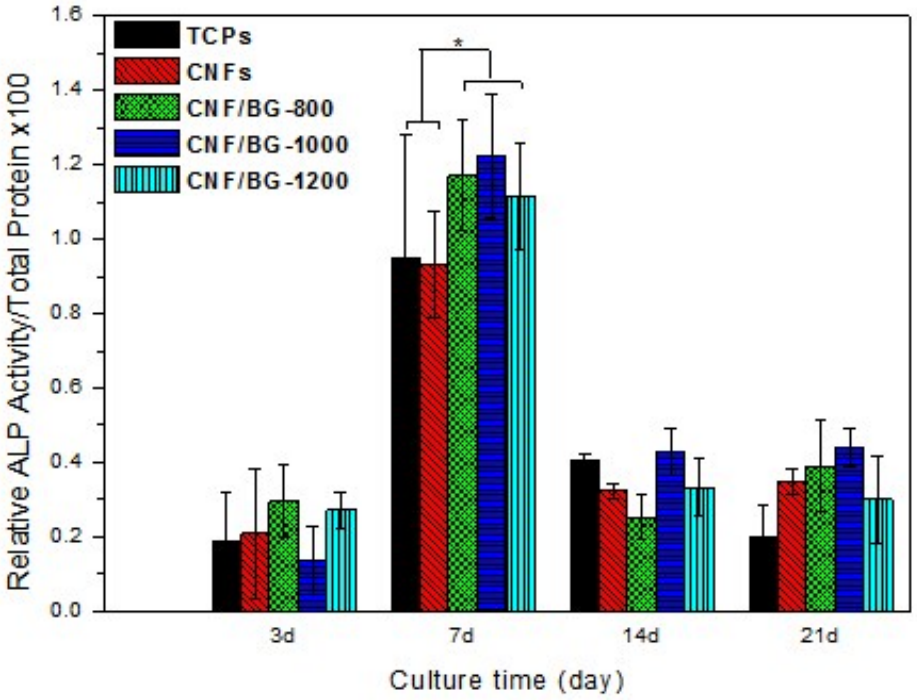

Fig. 9 ALP activity expression of MC3T3-E1 cultured on TCPs, pure CNFs and CNF/BG for various time. The results are represented as mean ± standard deviation for n = 3 ($P < 0.05$).

The ability of CNF/BG composites in enhancing osteogenic differentiation was investigated by measuring an early indicator of osteogenesis, i.e. the ALP activity expression of cultured MC3T3-E1 osteoblasts [46]. After the initial incubation period, as shown in Fig. 9, the ALP activity increased with longer culture time and reached the peak value after 7-day culture in all cases. The results demonstrated that all the

materials had certain ability in inducing osteogenic differentiation of MC3T3-E1 osteoblasts. In comparison with TCPs, the ALP expression on pure CNFs was only slightly different from that on TCPs, suggesting the CNFs themselves not having strong effect in enhancing osteogenic differentiation. On the contrast, the MC3T3-E1 osteoblasts showed distinctly high expression in ALP activity on all BG-containing CNFs composites, especially on CNF/BG-1000 composites, because the released ions from fast dissolved BG nanoparticles could act on the cells [47-49]. Clearly, the ALP activity on difference substrates closely related to their chemical compositions and dissolution rate of bioactive component.

Increasing evidences in literatures have indicated that ionic dissolution products from BG were a key factor in osteoblasts metabolism, proliferation and cell-cell and matrix-cell adhesion [13, 50]. The ionic dissolution products of BG nanoparticles from the CNF/BG composites into the culture medium would provide a favorable environment for MC3T3-E1 cells adhesion, proliferation and osteogenic differentiation. In other words, the incorporation of BG component into CNFs had endowed the material higher affinity to osteoblasts and higher ability in promoting osteogenic differentiation compared to pure CNFs. The thermal-based flexibility in preparing CNF/BG composites provided ability in regulating the morphology and structure of resulting composites, and a kind of promising substrate targeting for skeleton tissue regeneration was obtained. Noticeably, to produce this kind of CNF/BG composites in large scale for future application in bone repairing, prospectively, methods other than electrospinning were suggested according to some newly-published reports [51-54]. The methods such as centrifugal spinning and infusion gyration seemed more suitable to produce nanofibers with high production than electrospinning, and thus were able to accelerate the practical applications of nanofibrous substrates as biomaterials.

4. Conclusions

CNF/BG composites, which were produced from electrospinning of PAN-BG precursor mixed solution, enabled flexibility in regulating their physiochemical and biological properties by selecting different sintering temperatures. Under proper preparation parameters, the resulting CNF/BG composite could demonstrate favorable morphology and structure for osteoblasts by comprehensively enhancing its ability in inducing cell adhesion, proliferation, osteogenic differentiation and bone binding. The most important issue in achieving this ability was how to accelerate the ion-exchange and dissolution of BG component from CNF/BG composites. Benefiting from its small size of BG nanoparticles and the well exposure of BG nanoparticles to surrounding medium, in this study, the CNF/BG-1000 displayed strongest ability in enhancing biological behaviors of biomineralization and osteoblasts. Besides, the crystalline structure of BG nanoparticles obtained under different sintering temperatures might also influence the solubility of BG component in aqueous medium. Therefore, the CNF/BG composites prepared at the optimum sintering condition would be good candidates for bone repairing applications. The future application of techniques like centrifugal spinning or infusion gyration was envisioned quite hopeful in increasing the production of CNF/BG composites and able to promote their practical applications..

Acknowledgments

The authors are very pleased to acknowledge financial support from National Basic Research Program of China (2012CB933904), National Natural Science Foundation of China (No.51102008 and 51473016), the Research Fund for the Doctoral Program of Higher Education (No.20110010120014), and the Fundamental Research Funds for the Central Universities (No.ZY1106)

Notes and References

[a]*State Key Laboratory of Organic-Inorganic Composites, College of Materials Science and Engineering, Beijing University of Chemical Technology, Beijing 100029, P. R. China,* [b]*Changzhou Institute of Advanced Materials, Beijing University of Chemical Technology, Jiangsu 213164, P. R. China,* [c]*Beijing Laboratory of Biomedical Materials, Beijing University of Chemical Technology, Beijing 100029, P. R. China. Fax: +86-10-6441-2884; E-mail: jiaxl@mail.buct.edu.cn & caiqing@mail.buct.edu.cn*

[1] R. J. Minns, D. S. Muckle and J. E. Donkin, *Biomaterials*, 1982, 3, 81.

[2] T. J. Webster, M. C. Waid, J. L. McKenzie, R. L. Price and J. U. Ejiofor, *Nanotechnology,* 2004, 15, 48.

[3] K. L. Elias, R. L. Price and T. J. Webster, *Biomaterials*, 2002, 23, 3279.

[4] C. A. Bonino, L. Ji, Z. Lin, O. Toprakic, X. Zhang and S. A. Khan, *ACS Appl. Mater. Inter.*, 2011, 3, 2534.

[5] J. L. McKenzie, M. C. Waid, R. Shi and T. J. Webster, *Biomaterials,* 2004, 25, 1309.

[6] Q. Hu, Y. L. Li, G. H. Miao, N. R. Zhao and X. F. Chen, *RSC Adv.*, 2014, 4, 22678.

[7] J. G. Tie, T. A. Hannu, Y. K. Heimo and V. Eero, *Biomaterials*, 2001, 22, 1475.

[8] J. Luo, Y. Ling, X. Li, B. Yuan, F. Yu, W. H. Xie and X. F. Chen, *RSC Adv.*, 2015, 5, 79239.

[9] B. Michel and C. Mario, *Biomaterials*, 2005, 26, 3873.

[10] H. Alexander, J. Bojan, J. Djordje, F. Tobias, G. Peter, R. Stefan, S. Jochen, P. Wolfgang, L. Jonathan, J. Edouard and R. B. Aldo, *ACS Appl. Mater. Inter.*, 2014, 6, 2865.

[11] B. Han, X. H. Zheng, H. Y. Liu, X. L. Deng, Q. Cai, X. L. Jia, X. P. Yang, Y. Wei and G. Li, *J. Biomat. Sci. Polym.*, 2014, 25, 341.

[12] Q. Yang, G. Sui, Y. Z. Shi, S. Duan, J. Q. Bao, Q. Cai and X. P. Yang, *Carbon*, 2013, 56, 288.

[13] A. Hoppe, N. S. Guldal and A. R. Boccaccini, *Biomaterials*, 2011, 3, 2757.

[14] M. N. Rahaman, D. E. Day, B. S. Bal, Q. Fu, S. B. Jung and L. F. Bonewald, *Acta Biomater.*, 2011, 7, 2355.

[15] S. Q. Liu, W. Y. Gong, Y. M. Dong, Q. Hu, X. F. Chen and X. J. Gao, *RSC Adv.*, 2015, 5, 38830.

[16] H. Y. Liu, Q. Cai, P. F. Lian, Z. Fang, S. Duan, X. P. Yang, X. L. Deng and S. Ryu, *Mater. Lett.*, 2010, 64, 725.

[17] H. Y. Liu, Q. Cai, P. F. Lian, Z. Fang, S. Duan, S. Ryu, X. P. Yang and X. L. Deng, *Carbon*, 2010, 48, 2266.

[18] Y. H. Yu, Q. Yang, D. H. Teng, X. P. Yang and S. Ryu, *Electrochem. Commun.*, 2010, 12, 1187.

[19] X. L. Jia, T. H. Tang, D. Cheng, L. J. Guo, C. H. Zhang, Q. Cai and X. P. Yang, *RSC Adv.*, 2014, 4, 64299.

[20] L. Wang, Y. H. Yu, P. C. Chen, D. W. Zhang and C. H. Chen, *J. Power Sources*, 2008, 183, 717.

[21] M. A. Atwater, J. Phillips and Z. C. Leseman, *Carbon*, 2010, 48, 1932.

[22] H. Arstila, L. Hupa, K. H. Karlsson and M. Hupa, *J. Non. Cryst. Solids*, 2008, 35, 722.

[23] J. Ma, C. Z. Chen, D. G. Wang, X. G. Meng and J. Z. Shi, *Ceram. Int.*, 2010, 36, 1911.

[24] G. C. Marta, G. David and P. Kevin, *Biomaterials*, 2005, 26, 4903.

[25] E. G. Julie, R. J. Julian and L. H. Larry, *Biomaterials*, 2004, 25, 2039.

[26] C. H. Zhang, D. Cheng, T. H. Tang, X. L. Jia, Q. Cai and X. P. Yang, *J. Mater. Chem. B.*, 2015, 3, 5300.

[27] Y. Ohashi, *Phys. Chem. Miner.*, 1984, 10, 217.

[28] P. N. De Aza, Z. B. Luklinska, M. R. Anseau, F. Guitian and S. De Aza, *Biomaterials*, 2003, 8, 1437.

[29] P. N. De Aza, F. Guitian and S. De Aza, J. Valle, *Analyst.*, 1998, 123, 681.

[30] H. X. Yang and C. T. Prewitt, *Am. Mineral.*, 1999, 84, 929.

[31] T. Kokubo and H. Takadama, *Biomaterials*, 2006, 27, 2907.

[32] M. Y. Wu, Q. Y. Wang, X. Q. Liu and H. Q. Liu, *Carbon*, 2013, 51, 335.

[33] L. Zhang, W. W. Liu, C. G. Yue, T. H. Zhang, P. Li, Z. W. Xing and Y. A. Chen, *Carbon*, 2013, 61, 105.

[34] B. Marc and L. Jacques, *Biomaterials*, 2009, 30, 2175.

[35] R. Govindan, G. Suresh Kumar and E. K. Girij, *RSC Adv.*, 2015, 5, 60188.

[36] M. P. Marlin, M. Sylvain, M. C. Jean, P. Elodie and C. Jérôme, *J. Eur. Ceram. Soc.*, 2012, 32, 2765.

[37] N. Gupta, D. Santhiya, A. Aditya and K. Badra, *RSC Adv.*, 2015, **5**, 56794.

[38] P. X. Zhu, Y. Masuda and K. Koumoto, *Biomaterials*, 2004, 25, 3915.

[39] A. Bedilu, A. S. Allo and K. M. Rizkalla, *ACS Appl. Mater. Inter.*, 2012, 4, 3148.

[40] N. Viswanadham, S. Debnath, P. Sreenivasulu, D. Nandan, S. K. Saxenaac and A. H. Al-Muhtase, *RSC Adv.*, 2015, **5**, 67380.

[41] T. A. Ostomel, Q. H. Shi, C. K. Tsung, H. J. Liang and G. D. Stucky, *Small*, 2006, 2, 1261.

[42] Z. F. Lin, S. Q. Cao, X. Y. Chen, W. Wu, and J. S. Li, *Biomacromolecules*, 2013, 14, 2206.

[43] J. Y. Xin, T. C. Chen, Z. F. Lin, P. Dong, H. Tan and J. S. Li, *Chem. Commun.*, 2014, 50, 6491.

[44] B. Wang, Q. Cai, S. Zhang, X. P. Yang and X. L. Deng, *J. Mech. Behav. Biomed.*, 2011, 4, 600.

[45] A. Mathur, S. W. Moore, M. P. Sheetz and J. Hone, *Acta Biomater.*, 2012, 8, 2595.

[46] T. Olga, L. Sheyda, M. S. Molly, E. P. Alexandra and R. J. Julian, *Adv. Healthcar. Mater.*, 2014, 3, 115.

[47] E. Tsiridis, A. Bhalla, Z. Ali, N. Gurav, M. Heliotis, S. Deb and L. DiSilvio, Injury, *Int. J. Care Injured*, 2006, 37, 25.

[48] H. A. Declercq, R. M. H. Verbeeck, L. I. F. J. M. De Ridder, E. H. Schacht and M. J. Cornelissen, *Biomaterials*, 2005, 26, 4964.

[49] H. J. Prins, A. K. Braat, D. Gawlitta, W. J. A. Dhert, D. A. Egan, E. Tijssen-Slump, H. P. Yuan, P. J. Coffer, H. Rozemuller and A. C. Martens, *Stem Cell Res.*, 2014, 12, 428.

[50] A. C. M. Renno, M. R. Nejadnik, F. C. J. Van de Watering, M. C. Crovace, E. D. Zanotto, J. P. M. Hoefnagels, J. G. C. Wolke, J. A. Jansen and J. J. J. P. Van den Beucken, *Biomed. Mater.*, 2013, 8, 2365.

[51] X. W. Zhang, Y. Lu, *Polym. Rev.*, 2014, 54, 677.

[52] S. Mahalingam, M. Edirisinghe, *Macromol. Rapid Comm.*, 2013, 34, 1134.

[53] M. Khamforoush, T. Asgari, *Nano*, 2015, 10, 1550016.

[54] S. Q. Zhang, B. T. Karaca, S. K. VanOosten, E. Yuca, S. Mahalingam, M. Edirisinghe, C. Tamerler, *Macromol. Rapid Comm.*, 2015, 36, 14.

TOC

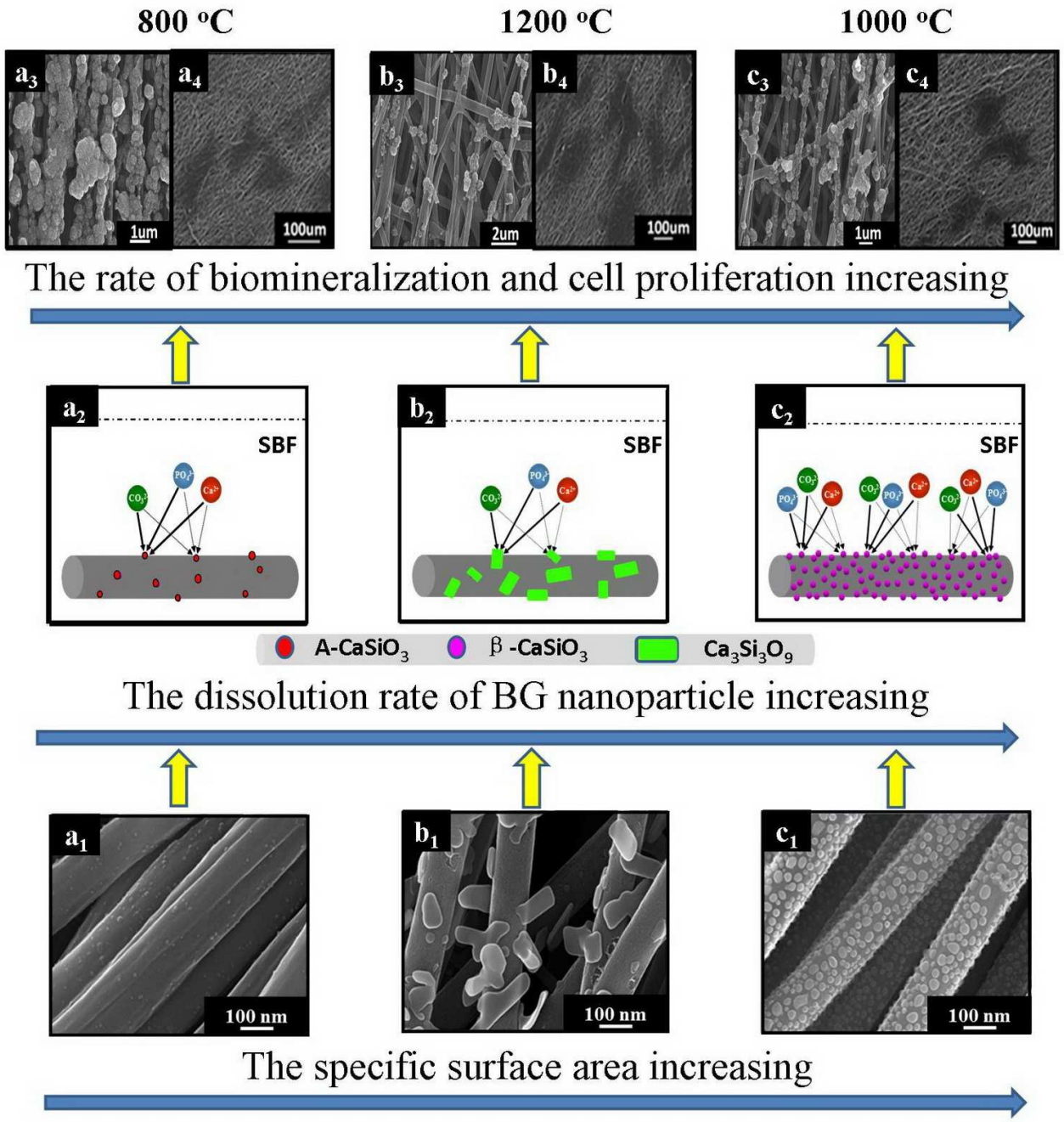

Mechanism and model of biomineralization behavior and cell culture of CNF/BG sintered at various temperatures.